PROTON COMPUTED TOMOGRAPHY

Kenneth M. HANSON

University of California
Los Alamos Scientific Laboratory
Los Alamos, NM 87545

ABSTRACT

The use of protons or other heavy charged particles instead of x rays in computed tomography (CT) is explored. The results of an experimental implementation of proton CT are presented. High quality CT reconstructions are obtained at an average dose reduction factor compared with an EMI 5005 x-ray scanner of 10:1 for a 30-cm-diameter phantom and 3.5:1 for a 20-cm diameter. The spatial resolution is limited by multiple Coulomb scattering to about 3.7 mm FWHM. Further studies are planned in which proton and x-ray images of fresh human specimens will be compared. Design considerations indicate that a clinically useful proton CT scanner is eminently feasible.

1. INTRODUCTION

Medical radiographic imaging took a giant leap forward with the introduction of the computed tomographic (CT) scanner. With it, radiologists were able to detect for the first time soft tissue abnormalities which differed only slightly ($\sim$ 1%) in density from the surrounding normal tissue. However, a new limit in density sensitivity has emerged which arises from the detection of a finite number of x rays by the CT scanners. The number of detected x rays may be increased by increasing the dose. However, it appears that radiologists are reluctant to increase the dose much above 10 rads in a CT examination. This self-imposed dose limit implies a corresponding limit in density sensitivity as long as x rays are used. Protons offer an alternative modality which can provide improved density resolution for a given dose. In this paper the advantages, disadvantages, and practicalities of the use of protons in medical CT imaging will be discussed. What can be said about protons may also be said of other heavy ions, such as deuterons, tritons, and alpha particles. These other ions will be discussed later.

2. PHYSICAL ASPECTS OF PROTON AND X-RAY RADIOGRAPHY

Figure 1 depicts the qualitative difference in the way protons and x rays sample the atoms in matter. The use of protons in medical imaging differs from that of x rays owing to the fact that protons are charged whereas x rays are not. Thus, in their passage through matter, protons interact with many atoms losing a small amount of energy in each interaction. A measurement of the total energy loss of a single proton provides information about a very large number of atoms, typically millions. Diagnostic x rays, on the other hand, are either scattered to wide angles or absorbed by each atom with which they collide. In x-ray radiography it is the attenuation of the unscattered x rays which is measured. The detection of the transmittance of a single x ray is representative of primary interactions of incident x rays with many atoms, typically thousands. A large number of x rays must be detected to attain the same accuracy in a pathlength measurement as the energy loss measurement of a single proton. However, the initial proton energy needed for the measurement is much larger, e.g., 200 MeV, than normal diagnostic x-ray energies, 70 keV. The dose advantage of protons is, therefore, not immediately obvious and must be based on an accurate calculation.

A calculation of the dose advantage has been performed in which ideally collimated, monochromatic beams and perfect detectors were assumed. It was further assumed that the water-like phantoms are placed in a water bolus. Protons which scatter

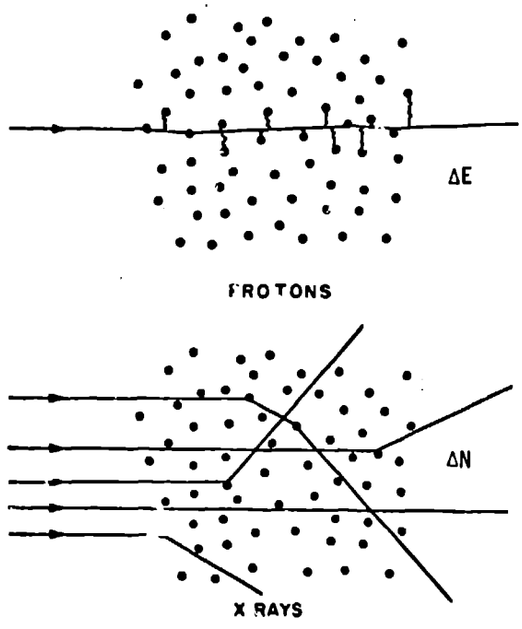

Figure 1

Schematic representation of the basic differences between protons and x rays in their interaction with atoms.

to large angles due to nuclear interactions contribute to the dose but cannot be used in the energy loss measurements. Table I summarizes the average doses obtained for a series of scans with 13 mm spacing for various sized phantoms. NEQ, the number of noise-equivalent quanta detected in the complete projection measurements, is a measure of the density sensitivity of a CT reconstruction [1]. An NEQ of 10^7 mm^{-1} implies an rms noise of 0.35% in a reconstruction with 1.5 x 1.5 mm^2 pixels using the Shepp and Logan algorithm [2]. One can see from Table I that the proton dose advantage increases as the phantom diameter gets larger. At a diameter of 30 cm (abdomen size) the dose advantage is about 6:1.

In their interactions with atoms, the protons undergo small angular deflections. This multiple Coulomb scattering leads to a divergence of a proton beam which is initially well collimated. The result is a limitation upon the spatial resolution which does not exist for x rays. As shown in Fig. 2, a 230-MeV proton beam will spread to a width of about 14 mm FWHM after passing through 30 cm of water.

TABLE I

COMPARISON OF PROTON AND X-RAY OPTIMUM AVERAGE DOSES REQUIRED TO PRODUCE RECONSTRUCTION WITH NEQ = 10^7 mm^{-1}

Diameter (cm)	Protons Energy (MeV)	Protons Avg. Dose (mrad)	X-Rays Energy (keV)	X-Rays Avg. Dose (mrad)	Proton Dose Advantage
10	130	8.2	55	20	2.4
20	190	30	80	94	3.1
30	230	65	100	370	5.7

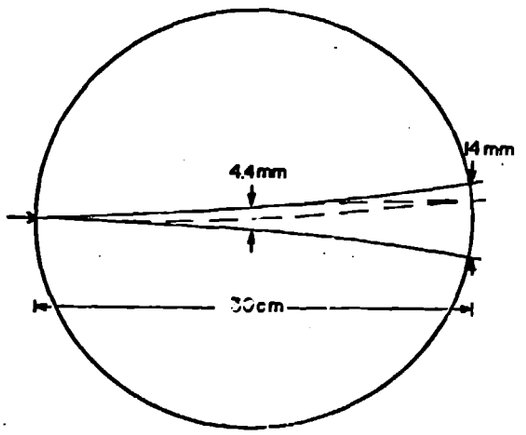

Figure 2

Spreading of a 230-MeV proton beam with a measurement of the exit position, dashed line, and without, solid line.

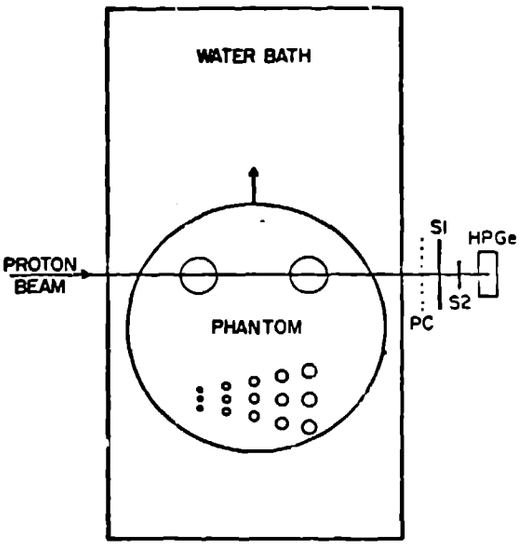

Figure 3

Schematic layout of proton CT experiment.

By constraining the exit position, one can reduce the maximum effective width of the beam envelope. This may be done without loss of dose advantage by measuring the exit position of each proton, one at a time. Further reduction of the effective width may be accomplished by measuring the angle, as well as the position, of the exiting protons [3]. To gain spatial resolution, the reconstruction algorithm might have to incorporate curved projection paths in an efficient way. Another way of coping with the lack of spatial resolution due to multiple Coulomb scattering is to use heavier charged particles. The principal advantage of light ions is that they are less affected by multiple Coulomb scattering than protons. For example, helium ions (alpha particles) with the same range as protons are deflected only half as much.

3. PROTON CT EXPERIMENT

An experiment was performed at LAMPF (Los Alamos Meson Physics Facility) to demonstrate that high quality CT reconstructions could be obtained with protons at significant dose savings compared with x-ray scanners. Experimental details not mentioned here may be found in Ref. 4. The general layout of the experiment is shown in Fig. 3. A secondary proton beam of variable energy was used. The beam energy bite was 0.4% and the beam width at entrance to the water bath was about 1.6 mm (FWHM). A hyperpure germanium detector (HPGe) measured the residual energy of each proton. The exit position of the proton was determined by the multiwire proportional chamber (PC). The scintillation counters S1 and S2 were used to trigger the data acquisition system. The residual energy and exit position of each proton event were recorded on magnetic tape by a PDP-11/45 computer for later analysis. The event rate was limited to about 700 events per second at a 50% deadtime by the CAMAC data acquisition system and the 6% LAMPF beam duty cycle. The CT scan was performed by translating the phantom across the stationary beam line. The phantom was then rotated before the next translation. A water bath was used to limit the required dynamic range.

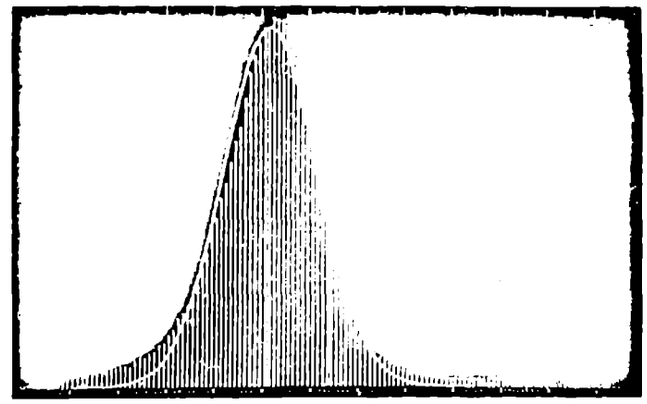

Figure 4

Residual energy distribution for a 30.5 cm water bath and an initial proton energy of 240 MeV. The mean residual energy is 36 MeV.

A typical HPGe energy spectrum is shown in Fig. 4. The width of the energy peak is dominated by straggling in the energy loss in the water bath. In the data analysis the energy peak is fit with a Gaussian function as shown to obtain the mean residual energy, which is, in turn, converted into a mean residual range. Stability runs have demonstrated that over a period of ½-hour, the stability in the residual range obtained in this manner was better than 2.5 g/cm^2 or more than 100 times smaller than the rms width of the range distribution. This implies the mean energy of the incident proton beam was stable to better than 0.006%.

In the data analysis the events were separated according to their exit position into 8 bins, each 2 mm wide. The residual range was calculated for the events in each of these bins. The set of residual ranges for a single exit bin obtained in a transverse scan of the phantom then comprise a single projection measurement. The filtered backprojection algorithm used to reconstruct the 2-D image simply backprojects the resulting projection along a straight line approximating the most probable curved path followed by the protons which exited in that particular bin. Calculations indicate that the errors made in this approximation are negligible. In the proton CT reconstructions presented here, the usual ramp filter has been rolled off using a Gaussian filter which drops to 0.5 at one half the Nyquist frequency of the reconstructions.

Two polyethylene phantoms were scanned. For a 30-cm-diameter phantom 52 million events were obtained in 45 hours of running time. Forty-two million events were obtained for a 20-cm-diameter phantom. The CT reconstructions of these phantoms are displayed in Fig. 5. In the 20-cm reconstruction 1 x 1 mm^2 pixels were used and for the 30-cm case 1.25 x 1.25 mm^2. The high and low contrast resolution sections of the phantoms were chosen to have nearly identical chemical composition as the background polyethylene to allow direct comparison with the x-ray scans shown in Fig. 6. The high contrast sections consist of polyurethane-filled holes with

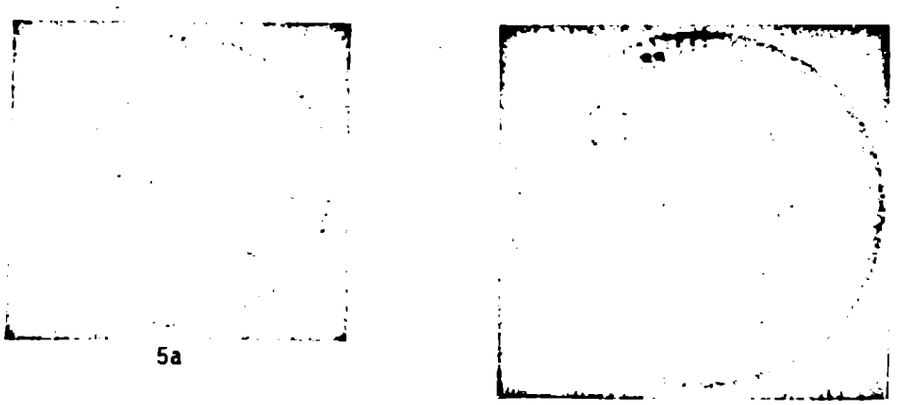

5a 5b

Figure 5

Proton CT reconstructions of a) 20-cm and, b) 30-cm phantoms at an average dose of about 0.6 rad for slice thickness of 1 cm.

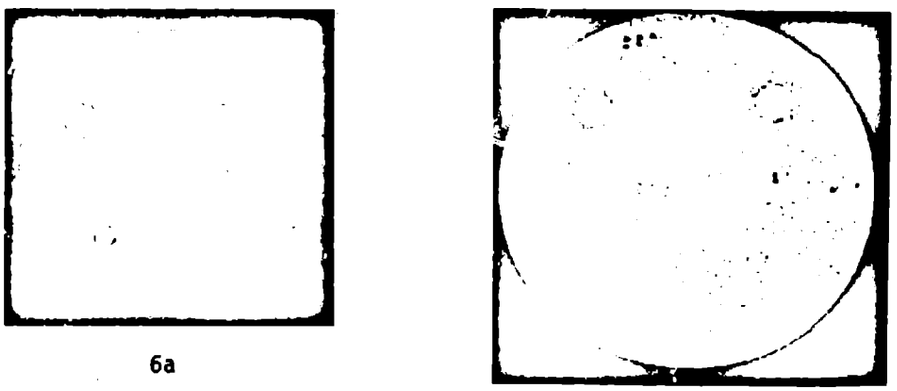

6a 6b

Figure 6

320 x 320 displays of normal EMI 5005 reconstructions of same phantoms shown in Fig. 5 at an average dose of 3.3 rad and 2.2 rad for 1-cm steps between slices.

diameters from 1 to 3 mm in 0.25 mm steps. Their contrast relative to the background is 10%. For the low contrast sections high density polyethylene dowels were press-fit into holes in the normal density polyethylene. The contrast of these dowels is about 1.8%. However, there is some variation in their contrast, particularly noticeable in the smaller diameter dowels in the 30-cm-diameter phantom. Comparison between Figs. 5 and 6 gives the qualitative impression that the density resolution of the x-ray scan is better than the proton scan for the 20-cm-diameter phantom while the proton scan is better for the 30-cm-diameter phantom. This is confirmed by the quantitative evaluation of the number of noise-equivalent quanta (NEQ), mentioned in Section 1. NEQ is inversely related to the low frequency content of the noise power. It can be shown that NEQ may be directly related to the signal-to-noise ratio for the detection of large, low density objects

TABLE II

COMPARISON: PROTON SCANS VERSUS EMI 5005 NORMAL SCANS

Scan	Diameter (cm)	Spatial Resolution (mm FWHM)	NEQ(10^7 mm^{-1})	Average Dose (rads)	Proton Dose Advantage
Proton	20	3.6	4.2	0.56	3.5
EMI	20	1.4	7.1	3.3	
Proton	30	3.8	2.5	0.60	10.0
EMI	30	1.8	0.91	2.2	

by an optimum observer [1]. Hence, it is a good measure of the density sensitivity of a reconstruction. Table II summarizes the NEQ obtained in the four scans.

The average doses for the four scans are given in Table II for a series of scans at 1 cm intervals. The proton doses are based on the number of incident protons required to produce the observed number of events for the specific experimental geometry used. The data acquisition deadtimes are not included in the dose calculations since these can be readily reduced in a proton scanner designed for low dose. The average EMI 5005 doses were scaled from measurements taken by Boyd, Margulis and Korobkin [5,6] and, perhaps, are accurate to only 20%. The dose advantages quoted in Table II were obtained by comparison of the ratio of NEQ to average dose for the two modalities. It is seen that for the 30-cm-diameter phantom the use of protons can result in a substantial (10:1) dose savings compared with the EMI 5005. This very promising feature of protons means that for a dose of about 1 rad, the proton CT technique should produce a reconstruction with a density resolution equivalent to that obtained in an EMI 5005 slow scan which delivers an average dose of about 9 rads and a peak skin dose of 22 rads.

The spatial resolution of the protons reconstructions, Fig. 5, is obviously worse than that of the EMI 5005 scans, Fig. 6. The full-width at half-maximums(FWHM) of the line spread functions of the reconstruction were estimated from the edge response at the nylon-polyethylene interface (upper left circle in Figs. 5 and 6b). It is seen from Table II that the proton spatial resolution is 2 to 2.5 times worse than that for the EMI 5005. While the proton spatial resolution is not too bad (the early GE CT/T scanners had comparable resolution), it would be advantageous to improve it. Methods for improvement were discussed in Section 2.

4. PROTON IMAGING OF BIOLOGICAL SPECIMENS

The energy loss method of proton radiography yields images which are related to the linear stopping power of protons, S, relative to some reference material, let us say water. In x-ray radiography the images are related to the linear attenuation coefficient, μ. While μ increases quite drastically with increasing atomic number Z, S depends rather weakly upon Z and, in fact, decreases with Z. Therefore, one expects images obtained with protons to be somewhat different than the traditional images obtained with x rays. For example, the water hole in the upper right quadrant of the proton reconstruction, Fig. 5b, is not much different than the polyethylene (1.7%) whereas in the x-ray picture, Fig. 6b, it is substantially different (10%). Thus, it is legitimate to ask whether or not proton images would be useful in diagnostic medicine.

Fortunately, several experiments have already shown that anatomical structures and abnormal tissues can be visualized with heavy charged particles. Steward and Koehler [7-10] have shown that the presence of lesions in the brain and breast may be readily detected using the proton shadowgraph method with film as the detector. The very high contrast inherent in this method, first demonstrated by Koehler [11], made it possible to visualize the lesions in the directly exposed film. Such visualization is not usually obtained with normal x-ray shadowgraphs since their contrast is too low. It should be further pointed out that Steward and Koehler's proton images were obtained at modest dose levels (< 1 rad). Similar results have been obtained at Argonne National Laboratory using a scintillation counter or a detector [12]. Investigators at the Lawrence Berkeley Laboratory [13] are making a comparison between x-ray and heavy ion (carbon) radiographs of various human specimens. Initial results indicate that tumors can be detected with the carbon radiographs taken at doses less than 100 mrad as well as with the x-ray radiographs. The first CT reconstruction with charged particles was realized by Crowe, Budinger, and their collaborators [14]. Their alpha scan of a human head demonstrated that a wealth of anatomical information can be obtained in charged particle radiography.

While the above-mentioned results are very encouraging, a detailed comparison of the contrast of specific types of lesions between x-ray and charged particle radiography remains to be made. At LAMPF we plan to perform such a detailed comparison for a variety of fresh (unfixed) human specimens. The results of a side-by-side comparison of x-ray and proton CT reconstructions will be correlated with pathological findings. This study should provide a measure of the utility of protons in diagnostic imaging. Through the use of special data acquisition hardware, we expect to reduce the scan time for 60 million events to less than 30 minutes, which is satisfactory for fresh specimens.

Contrast agents are routinely used in x-ray medical imaging. The rapid dependence of μ upon Z permits a very small concentration of these high Z agents to be seen in the x-ray radiographs. The weak Z dependence of the proton stopping power precludes the use of such contrast agents in proton radiography. This may prove to be a serious deficiency of charged particle radiography. However, this detriment must be weighed against the improved density resolution (per unit dose) possible with charged particles and the as yet unknown response of charged particles to abnormal tissue.

5. FUTURE POSSIBILITIES AND PRACTICALITIES

Let us consider some of the practicalities of implementing a heavy charged particle CT scanner for clinical use. Table III compares the characteristics of several heavy ions which might be used. It is seen that the relative dose advantage (taken from Ref. 3 for a 25-cm-dia scan and arbitrarily normalized to 10 for protons) is actually maximized for a tritium beam and drops considerably for ions as heavy as carbon. The relative spatial resolution (Ref. 3, arbitrarily normalized to unity for protons), on the other hand, continues to improve as the atomic weight increases. The ultimate choice for a CT scanner may depend upon several design considerations. However, tritium offers the attractive feature of the best dose efficiency with moderately improved spatial resolution compared with protons.

In the present discussion we will concentrate on the feasibility of scanning a patient in 10s with a proton beam. The objective would be to accumulate 10^8 events with which to make a CT reconstruction. For a 30-cm-diameter specimen, approximately 1 rad would be delivered for a 1-cm thick slice.

The charged particle accelerator and beam delivery system represent, perhaps, the biggest departure from a conventional x-ray CT scanner. The accelerator should be able to supply the maximum energy listed in Table III in order to accommodate

TABLE III

Particles	Maximum Energy (50 g/cm^2) (MeV)	Rigidity (Telsa-meter)	$\frac{\sigma_R}{R}$ (%)	Relative Dose Advantage	Relative Spatial Resolution
P	300	2.7	1.1	10.0	1.0
d	400	4.3	0.81	11.6	.73
t	470	5.7	0.67	12.4	.64
α	1200	5.4	0.55	6.6	.50
C^{12}	7000	8.0	0.30	2.4	.28

specimens up to 45 g/cm^2 thick. The corresponding rigidity (magnetic field x bending radius) indicates the necessary radius of a circular accelerator of given magnetic field strength. For example, at a field of 1T (10 kilogauss), which is easy to achieve with standard magnets covering 2/3 of its circumference, a proton accelerator would have a diameter of 8.1 m. Larger diameters would be required for the heavier particles unless superconducting magnets were used. Superconducting magnet technology, although not as yet commonplace, is becoming very reliable. The available magnetic fields of between 4 to 6T could make possible a compact accelerator which would fit in any hospital. If space requirements were not a problem, conventional iron-core magnets might be less expensive.

The design of a diagnostic proton accelerator has been considered by Martin et al. [15]. The unique requirements of a diagnostic proton beam of low beam intensity, small phase space and slow acceleration help reduce costs. An H^- beam was considered for ease of extraction. The capital cost of the production model of such an accelerator is presently estimated to be $400 K [15]. In contrast, the design study made by Lawrence Berkeley Laboratory and the Arizona Medical Center [17] concluded that a dedicated medical ion accelerator would cost about $7 M. However, the latter design was predicated upon the moderate beam intensity requirements of radiation therapy and did not take into account possible reductions in cost arising from the production of several such accelerators. Improvements in accelerator technology [18] may also bear on the ultimate cost of accelerators for diagnostic purposes.

The CT scanning of a supine patient can be achieved with a beam delivery system as shown in Fig. 7. The small phase space of the beam implies a minimum of focussing elements (quadrupole doublets). The drawing assumes a bending radius of 1 m which is possible for all the particles listed in Table III (except for C^{12}) if superconducting magnets are used. The scanning magnets would sweep the beam in the plane perpendicular to the page to produce a fan-beam sampling geometry. To obtain 300 projection measurements in 10s, the magnet would have to follow a 15 Hz sawtooth waveform with a peak-to-peak amplitude of 2T for the tritium beam. Rotation of the entire beam delivery system about the patient in 10s should not be difficult since the centripetal acceleration is less than 1/20 g. Again, the small phase space of the beam should make it possible to use magnets of small dimensions.

The detector system envisioned for a fast proton CT scanner would exclusively use plastic scintillators and high speed photomultipliers. With these detectors, time resolutions of better than 10 ns are easily achieved. At the 10 MHz average data rate needed to acquire 10^8 events in 10s, the probability of an accidental coincidence between two events (thus voiding both events) would be less than 10%. These

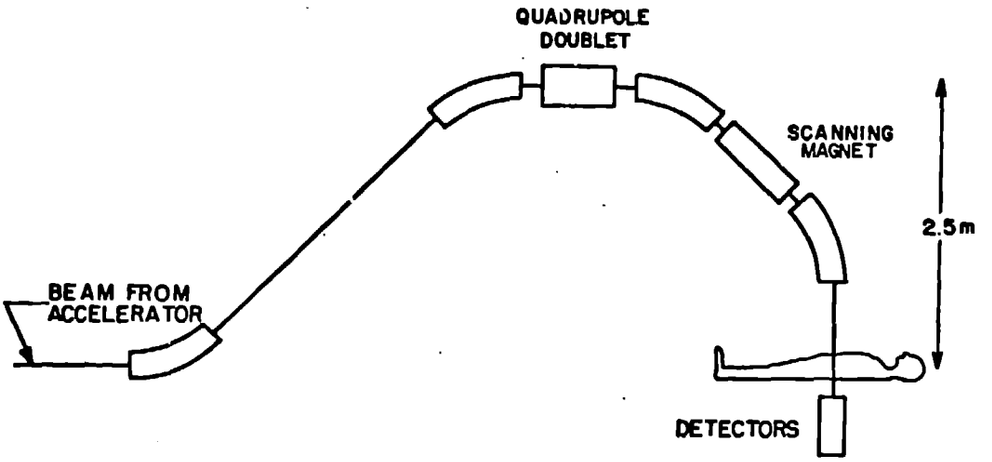

Figure 7

A possible beam delivery system.

detectors are somewhat simpler to operate than the usual scintillation counters used in x-ray scanners since they do not require very good gain stability. If 1.5 mm wide scintillator strips were used to measure the exit position of the protons, approximately 300 counters would be required. The residual range of the exiting protons would be determined with a scintillator range telescope which spanned the entire width of the patient. A counter thickness of 3 mm might be used for protons. A total variation of 30 g/cm^2 in the residual range could be accommodated with 100 counters.

At first sight the data handling problems associated with a 10 MHz data rate appear formidable. However, upon closer inspection, these problems are found to be soluble with present-day technology with only a modest amount of multiplexing and parallel processing. The encoding of the scintillator data to form a binary address can be done in about 40 ns with ECL logic circuitry. Two-dimensional histograms of the correlation between the exit position and residual range can be accumulated as the data come in at a 10 MHz rate using Schottky TTL logic components. The peaks in the range curves would be determined with parallely operating Schottky TTL microprogramming facilities (Advanced Micro Devices 2900), each responsible for the range curve associated with a given exit position. The end result would be the projection data needed for reconstruction, which might be performed on a minicomputer.

In conclusion, the construction of a 10-second heavy charged particle CT scanner appears feasible. Although the cost of such a scanner has not been estimated, it is clear that it would be substantially more expensive than the x-ray CT scanners now available. Justification for this extra cost can only be based upon the performance of heavy charged particle scanners in their diagnostic task of identifying and localizing soft-tissue abnormalities. If particle accelerators are installed in hospitals for other uses, such as isotope production or therapy, the add-on cost of a charged particle CT scanner would be significantly reduced. It is possible that the improved density resolution provided by these scanners for a given dose level in combination with peculiarities in their imaging of lesions could ultimately make them worthwhile.

ACKNOWLEDGEMENTS

The author would like to acknowledge helpful discussions with Rodney Brooks, David Brown, David Bowman, William Holley, Stephen Kramer, Donald Machen, Dr. William Steward and Donald Swenson.

REFERENCES

[1] K. M. Hanson: Detectability in computed tomographic images, to be published.
[2] L. A. Shepp and B. F. Logan: The Fourier reconstruction of a head section, IEEE Trans. Nucl. Sci. NS-21 (1974) 21-43.
[3] R. H. Huesman, A. H. Rosenfeld, and F. T. Solnitz: Comparison of heavy charged particles and x-rays for axial tomographic scanning, LBL-3040, 1975.
[4] K. M. Hanson et al.: The application of protons to computed tomography, IEEE Trans. Nucl. Sci. NS-25 (1978) 657-660.
[5] D. P. Boyd, A. R. Margulis, and M. Korobkin: Comparison of translate-rotate and pure rotary CT body scanners, Proc. SPIE 127 (1978) 280-285.
[6] D. P. Boyd: private communication.
[7] V. W. Steward and A. M. Koehler: Proton beam radiography in tumor detection, Science 173 (1973) 913-914.
[8] V. W. Steward and A. M. Koehler: Proton radiographic detection of strokes, Nature 245 (1973) 38-40.
[9] V. W. Steward and A. M. Koehler: Proton radiography in the diagnosis of breast carcinoma, Radiol. 110 (1974) 217-221.
[10] V. W. Steward and A. M. Koehler: Proton radiography of a human brain tumor within the skull: a preliminary report, Surg. Neurology 2 (1974) 283-284.
[11] A. M. Koehler: Proton radiography, Science 160 (1968) 303-304.
[12] S. L. Kramer, R. L. Martin, D. R. Moffett, and E. Colton: Application proton radiography to medical imaging, presented at the 1st Int. Seminar on the Use of Proton Beams in Radiation Therapy, Moscow, 1977.
[13] C. A. Tobias, E. V. Benton, and M. P. Capp: Heavy-ion radiography, LBL-5610 (1977) 164-186.
[14] K. M. Crowe, T. F. Budinger, J. L. Cahoon, V. P. Elischer, R. H. Huesman, L. L. Kanstein: Axial scanning with 900-MeV alpha particles, IEEE Trans. Nucl. Sci. NS-22 (1975) 1752-1975.
[15] R. L. Martin, M. Foss, J. Moenich, and R. Fari: The proton diagnostic accelerator, IEEE Trans. Nucl. Sci. NS-22 (1975) 1802-1804.
[16] R. L. Martin: private communication
[17] E. J. Lofgren et al.: Dedicated medical ion accelerator design study: final report, LBL-7230 (1977).
[18] D. A. Swenson: Alternating phase focussed linacs, Particle Accelerators 7 (1976) 61.